

## Pharmacokinetic Analysis of Dynamic $^{18}\text{F}$ -FMISO PET Data in Non-small Cell Lung Cancer

Jazmin Schwartz<sup>1</sup>, Milan Grkovski<sup>1</sup>, Andreas Rimner<sup>2</sup>, Heiko Schöder<sup>3</sup>, Pat B. Zanzonico<sup>1</sup>, Sean D. Carlin<sup>3</sup>, Kevin D. Staton<sup>3</sup>, John L. Humm<sup>1</sup>, Sadek A. Nehmeh<sup>4</sup>

<sup>1</sup>Department of Medical Physics, Memorial Sloan Kettering Cancer Center, New York, New York

<sup>2</sup>Department of Radiation Oncology, Memorial Sloan Kettering Cancer Center, New York, New York

<sup>3</sup>Department of Radiology, Memorial Sloan Kettering Cancer Center, New York, New York

<sup>4</sup>National Center for Cancer Care and Research, Doha, Qatar

Corresponding Author:

Jazmin Schwartz, PhD

Department of Medical Physics

Memorial Sloan Kettering Cancer Center

1275 York Avenue

New York, NY 10065

Phone: 212-639-2833

FAX: 212-717-3010

Email: [schwarzj1@mskcc.org](mailto:schwarzj1@mskcc.org)

Word count (Main text):

Running Title:  $^{18}\text{F}$ FMISO Pharmacokinetics in NSCLC

## ABSTRACT

Hypoxic tumors exhibit increased resistance to radiation, chemical, and immune therapies.  $^{18}\text{F}$ -fluoromisonidazole ( $^{18}\text{FMISO}$ ) PET is a noninvasive, quantitative imaging technique used to evaluate the magnitude and spatial distribution of tumor hypoxia. In this study, pharmacokinetic analysis (PKA) of  $^{18}\text{FMISO}$  dynamic PET (*dynFMISO*) extended to 3 hours post-injection is reported for the first time in stage III-IV non-small cell lung cancer (NSCLC) patients.

**Methods** Seventeen patients diagnosed with NSCLC underwent 2 PET/CT scans (1-3 days apart) before radiation therapy (RT): a 3-min static  $^{18}\text{FDG}$  and a dynamic  $^{18}\text{FMISO}$  scan lasting  $168\pm 15$  min. The latter data were acquired in 3 serial PET/CT dynamic imaging sessions, registered with each other and analyzed using pharmacokinetic-modeling software. PKA was performed using a 2-tissue, 3-compartment irreversible model and kinetic parameters were estimated for the volumes-of-interest (VOI) determined using co-registered FDG images for both the VOI-averaged and voxel-wise time-activity curves (TACs) for each patient's lesions, normal lung and muscle.

**Results** We derived average values of  $^{18}\text{FMISO}$  kinetic parameters for NSCLC lesions as well as for normal lung and for muscle. We also investigated the correlation between the trapping rate ( $k_3$ ) and (a) delivery rate ( $K_1$ ), (b) influx rate ( $K_i$ ) constants and (c) and tissue-to-blood activity concentration ratios (TBR) for all tissues. Lesions had trapping rates 1.6 times larger, on average, than those of normal lung and 4.4 times larger than those in muscle. Additionally, for almost all cases,  $k_3$  and  $K_1$  had a significant strong correlation for all tissue types. The  $TBR-k_3$  correlation was less straightforward, showing a moderate to strong correlation for only 41% of lesions. Finally,  $K_1-k_3$  voxel-wise correlations for tumors were varied, but negative for 76% of lesions, globally exhibiting a weak inverse relationship (average  $R = -0.23\pm 0.39$ ). However, both normal tissue types exhibited significant positive correlations for >60% of patients, with 41% having moderate to strong correlations,  $R > 0.5$ .

**Conclusion** All lesions showed distinct  $^{18}\text{FMISO}$  uptake. Variable  $^{18}\text{FMISO}$  delivery was observed across lesions, as indicated by the variable values of the kinetic rate constant  $K_1$ . Except for three cases, some degree of hypoxia was apparent in all lesions based on their non-zero  $k_3$  values.

**Key words:** Non-small cell lung cancer; hypoxia; <sup>18</sup>F-fluoromisonidazole; compartmental analysis; pharmacokinetic analysis

## INTRODUCTION

Lung cancer is the malignancy with the highest mortality for both men and women. Approximately 70% of these patients are diagnosed with “nonsquamous” non-small cell lung cancer (NSCLC). The 5-year survival of patients treated with surgery alone is 73%, 58% and 13% for stages IA, IB and IIIA NSCLC, respectively. Treatment failures are usually associated with distant metastatic recurrences. Even with multimodality treatment (including surgery, chemotherapy, and radiotherapy) in non-responders to neoadjuvant chemotherapy, the 2-year local control and survival rates are less than 60% (1). Tumor hypoxia has been shown to be an independent prognostic marker in several malignancies, including NSCLC (2). Hypoxic tumors, generally express a more aggressive phenotype and are radioresistant and thus have an increased likelihood of loco-regional recurrence, distant metastasis, and poor overall outcome (3,4). Nordmark et al. showed, in fact, that the most predictive factor of survival in head-and-neck cancer (HNC) was the proportion of the measurements in each lesion with  $pO_2$  less than 2.5 mmHg; a steep decline in survival was observed when more than 20% of a lesion’s measurements had  $pO_2 < 2.5$  mmHg (5). In NSCLC, 38% of patients had lesions with >20% of the measurements having  $pO_2 < 2.5$  mmHg (6). Potential treatment strategies for overcoming tumor hypoxia and improving local control rates include the use of radiosensitizing drugs and biological image-guided dose escalation to hypoxic tumor sub-regions (7-11).  $^{18}F$ MISO PET has been widely investigated as a non-invasive method for detecting tumor hypoxia in several solid tumors, including NSCLC (2,3). Rajendran *et al.*, building on previous work in animals by Koh *et al.*, used  $^{18}F$ MISO uptake at 120min post-injection to quantify tissue hypoxia; they defined a tumor

fractional hypoxic volume (FHV) by including voxels in the tumor image with TBRs greater than 1.4 (12,13). However, the application of  $^{18}\text{F}$ MISO to assess the FHV in NSCLC has yet to be investigated. Different TBRs and tumor-to-muscle and tumor-to-mediastinum activity concentration ratios (TMRs and TMeRs, respectively) have been proposed as semi-quantitative criteria for delineating hypoxic tumor volumes (3,12-14); for example, Eschmann et al. showed that a TMeR greater than 2 was a predictive factor for local recurrence in lung cancer. However, Thorwarth demonstrated that no single ratio threshold in the late  $^{18}\text{F}$ MISO images may be sufficient to accurately define the spatial distribution of tumor hypoxia (3,15). Instead, they suggested that *PKA* of dynamic  $^{18}\text{F}$ MISO PET images should be used to extract local hypoxia and perfusion characteristics of tumor tissue (15). In a separate study, Wang and co-workers argued that the physiologic clearance of  $^{18}\text{F}$ MISO from highly perfused normal tissue may result in *TBRs* comparable to those in a tumor at the time of patient imaging (16). Eschmann identified 3 types of TACs, representing rapid washout, intermediate or delayed washout, or continuing accumulation, respectively, which correlated with treatment outcome after radiotherapy (3). In particular, an accumulation-type curve, a high  $^{18}\text{F}$ MISO SUV, and a high TMeR at 4h after injection were highly suggestive of incomplete response to treatment (3).

In this study, we used compartmental modeling to investigate the presence and extent of tumor hypoxia, as measured by  $^{18}\text{F}$ MISO PET, in a cohort of NSCLC patients, prior to treatment. In addition, tumor parametric maps of hypoxia surrogate ( $k_3$ ,  $K_i$  and *TBR*) and delivery ( $K_1$ ) metrics were derived and correlations among these parameters evaluated.

## **MATERIALS AND METHODS**

### **Patients Cohort**

Sixteen NSCLC (10 males and 6 females; age  $66\pm 12$  yrs) scheduled for definitive RT were included in this study after. The institutional IRB approved this study and all subjects signed a written informed consent. Patient characteristics are summarized in Table 1. The mean tumor volume of the sixteen patients included in this study was  $\sim 18.8$ cc (range, 1.7–147.0cc). All patients underwent a pre-therapy FDG PET/CT scan for RT planning. A baseline  $^{18}\text{F}$ MISO PET/CT scan was then performed up to three days following the FDG study.

### **FDG PET/CT**

Patients were required to fast for at least 6 h before intravenous injection with  $429\pm 16$  MBq of  $^{18}\text{F}$ FDG. Patients underwent  $^{18}\text{F}$ FDG PET/CT at  $60\pm 10$  min post-injection while immobilized in an RT-simulation cradle. An additional 3-min free-breathing  $^{18}\text{F}$ FDG scan was acquired over one PET field-of-view centered over the primary lesion, followed by a low-dose 4DCT (120kVp, 10 mA, tube rotation 0.5sec). A time-averaged CT ( $CT_{avg}$ ) was generated retrospectively and used for attenuation correction of free-breathing PET images. PET/CT images were acquired on a GE Discovery ST PET/CT scanner in 3D mode (GE Health Care, Waukesha, WI). PET emission data were corrected for attenuation, scatter, and randoms, and iteratively reconstructed using standard clinical parameters (16 subsets, 2 iterations, transaxial post-filter Gaussian filter 6.0mm FWHM, Heavy 3 point-smoothing axially).

## **FMISO PET/CT**

Patients were injected intravenously with an average of  $346 \pm 33$  MBq (range=242-382 MBq)  $^{18}\text{F}$ FMISO simultaneously with the start of data acquisition (bolus duration ~5sec). No fasting was required prior to the  $^{18}\text{F}$ FMISO injection. The  $^{18}\text{F}$ FMISO was synthesized in our facility using a commercially available cassette (GE Health Care, Waukesha, WI), with radiochemical purity of at least 95% by HPLC. The patients were scanned while supine on a flat-top couch insert on a GE Discovery 690 PET/CT Scanner with Time-of-Flight (GE Health Care, Waukesha, WI), and immobilized in the RT-simulation cradle. A dynamic  $^{18}\text{F}$ FMISO PET (FMISO-1) acquisition over one bed position (centered over the primary lesion) was performed and consisted of  $12 \times 10$ sec,  $8 \times 60$ sec, and  $7 \times 300$ sec frames (total duration=45 min). This was followed by two additional 10-min static image acquisitions: FMISO-2 at  $95 \pm 12$ min (range, 79-98 min) and FMISO-3 at  $168 \pm 15$  (range, 146-181min) post-injection. A low-dose 4DCT (same acquisition parameters as for FDG PET/CT study) scan preceded each of the three  $^{18}\text{F}$ FMISO PET sessions; the corresponding  $CT_{avg}$  was used for attenuation correction and image registration purposes. All  $^{18}\text{F}$ FMISO PET images were reconstructed using (20 subsets, 2 iterations, trans-axial Gaussian post-filter 6.4 mm FWHM, Heavy 3 point-smoothing axially).

### **Image Post-Processing and Preliminary Measurements**

The PET tumor volumes from FDG, FMISO-2, and FMISO-3 were co-registered to that of FMISO-1 by means of their corresponding  $CT_{avg}$  images, using the GE Advantage Workstation rigid registration software tool (General Electric Advantage

Workstation v4.7). For patients exhibiting multiple lesions, the registration process and the following processing were performed separately for each lesion. The FMISO-2 and FMISO-3 image sets were decay corrected to the start time of the FMISO-1 acquisition, and then these three data sets were merged using PMOD (v.3.609 PMOD Technologies, Inc., Zurich, CH) into one dynamic image set (*dynFMISO*).

Since the heart was within the imaged field-of-view, image-derived input functions (IF) were used for this study. Recent work by Nguyen-Kim has shown that, in NSCLC, the bronchial contribution to pulmonary circulation is higher than the pulmonary (17). Thus, a VOI was drawn over the aortic arch on the  $CT_{avg}$  image, well within the edges of the structure in order to avoid spill-over effects (Fig. 1A *left*), then superimposed on the frames of the *dynFMISO* image set (Fig. 1A *right*). The TACs of the 25 VOI voxels with highest activity concentration during the second frame were averaged to obtain the IF (Fig. 1C *green*).

Tumor volumes were delineated on the registered FDG (Fig. 1B *mid*) image and then segmented using a 50%-of-maximum threshold. The background in the FDG images was at least 10 times smaller than the uptake in the lesions. Thus, it was not necessary to account for it as a caveat for adjusting the threshold. A fused PET/CT was used to ascertain that the VOI was within the tumor on  $CT_{avg}$ . The VOI thus derived,  $VOI_{Tumor}$ , was then superimposed on the frames of the *dynFMISO* image set (Fig. 1B *right*). Voxel-wise TACs were obtained for all voxels within the  $VOI_{Tumor}$ , and then averaged to provide a mean  $VOI_{Tumor}$  TAC ( $TAC_{Avg}$ ). Finally, two additional VOIs were drawn for each patient: (1)  $VOI_{Normal}$ , an ellipsoid drawn over the contralateral normal lung; and (2)  $VOI_{Muscle}$ , drawn over muscle in the latissimus dorsi region (Fig. 1B



blue/red respectively). PKA was carried out on the mean TAC of each region ( $TAC_{Normal}$  and  $TAC_{Muscle}$ , Fig. 1C).

Voxel-wise TBRs were calculated for the last frame time,  $t_{late}$ , for each VOI:

$$TBR = \frac{AC_{Late}}{IF_{Late}} \quad (1)$$

where  $AC_{Late}$  and  $IF_{Late}$  are the last-frame activity concentrations for a given voxel TAC and IF, respectively. The maximum TBR ( $TBR_{max}$ ) was then determined. Based on previous work, the tumor hypoxic volume (HV) was defined as the volume containing voxels with  $TBRs > 1.2$  (18). The FHV was calculated as:

$$FHV = \frac{HV}{Lesion\ Volume} \quad (2)$$

In addition, the TACs of all voxels within the HV were averaged to obtain  $TAC_{FHV}$  for each lesion and PKA carried out of each. For each VOI, the last-frame  $SUV_{bw}$  was also calculated:

$$SUV_{bw} = \frac{AC_{Late}}{Injected\ Dose / bw} \quad (3)$$

where  $bw$  is the body weight (kg). Finally, TMR for each lesion is calculated as  $TMR = Lesion\ TBR / Muscle\ TBR$ .

## Pharmacokinetic Analysis

The TAC from dynamic PET data,  $C_{PET}(t)$ , represents the averaged activity concentration in a volume (voxel or VOI) at acquisition time  $t$  post-injection and is modeled by

$$C_{Model}(t) = (1 - vB) \times (C_1(t) + C_2(t)) + vBC_p(t) \quad (4)$$

Every volume, whether a voxel or VOI, is heterogeneous, comprised of various tissues and vascular components. The fraction of the vascular space in a volume,  $vB$ , accounts for the activity arising from the blood within the volume and  $(1-vB)$  represents the fraction of activity in tissue which is extravascular. The contributions to the measured  $C_{PET}(t)$  in a given volume are those from tracer which is: (1) circulating within the plasma ( $p$ ), ( $C_p(t)$ ), (2) extracted from plasma into tissue and remaining unbound/free ( $C_1(t)$ ) and (3) irreversibly bound, ( $C_2(t)$ ) (19,20). Bruehlmeier et al. have shown that the percent of metabolic degradation of  $^{18}F$ MISO is negligible, so metabolite correction is unnecessary. The rate of change of the activity in a given compartment, as a function of time, is a linear combination of the fluxes, scaled by rate constants, into and out of it.

This relationship may be described via coupled differential equations:

$$\frac{dC_1(t)}{dt} = k_1 C_p(t) - (k_2 + k_3) C_1(t) \quad (5)$$

$$\frac{dC_2(t)}{dt} = k_3 C_1(t) \quad (6)$$

The pharmacokinetic rate constants  $K_1$  and  $k_2$  represent the rate of transport from plasma into and the efflux rate out from the unbound compartment, respectively, while  $k_3$  is the rate at which  $^{18}F$ MISO is trapped. Therefore,  $k_3$  is often considered a possible surrogate hypoxia metric (21).

Modeling was performed using PMOD with a 2-tissue, 3-compartment (plasma, free, bound) model with irreversible binding ( $k_4=0$ ). Fitting was performed with Levenberg–Marquardt weighted least-squares (WLS) optimization to obtain the parameters  $K_1$ ,  $k_2$ ,  $k_3$  and  $vB$  (22,23). The weights were obtained by (16):

$$w_i = \frac{1}{\sigma_i^2}, \sigma_i = c \sqrt{\left( \frac{C_{PET}(t_i)}{\Delta t_i \times e^{-\lambda t_i}} \right)}, \quad (7)$$

where  $c$  (0.064 as we previously calculated (24) ) is the scaling factor,  $\Delta t_i$  the frame duration,  $C_{PET}(t_i)$  the decay-corrected activity concentration at time  $t_i$ , and  $\lambda = \ln(2)/T_{1/2}$  the decay constant.

The PKA results were compared for tumor, normal lung and muscle VOIs voxel-wise and averaged over the whole target volume (i.e.  $TAC_{Avg}$ ). The influx rate ( $K_i = k_1 k_3 / (k_2 + k_3)$ ) was also calculated, as it has been suggested as a possible surrogate measure of hypoxia (16,21,25).

## RESULTS

Figure 2A shows representative model curves,  $C_{Model}(t)$ , and the corresponding unbound and trapping compartment curves,  $C_1(t)$  and  $C_2(t)$  (Fig. 2B and 2C, respectively), for  $VOI_{Tumor}$  (black),  $VOI_{Normal}$  (blue) and  $VOI_{Muscle}$  (red) average TACs, respectively.

PKA results for the tumors'  $TAC_{Avg}$  for the 16 patients (34 lesions) and values of TBR, lesion volume, and maximum  $SUV_{bw}$  are tabulated in Tables 2 and 3 and Supplement Tables 1 and 2. The average values ( $\mu$ ) and corresponding standard deviations (SD) and ranges for each parameter: (1)  $vB=0.15\pm 0.10$  (0.01-0.45); (2)  $K_1=0.15\pm 0.06$  (0.05-0.25) mL/min/cc; (3)  $K_1/k_2=0.69\pm 0.23$  (0.18-1.14); and (4)  $k_3=0.0041\pm 0.0045$  (0.00-0.021) min<sup>-1</sup>. The average TBR across lesions was  $1.80\pm 1.45$  (0.54-7.97). The results for normal lung and muscle are summarized Tables 4 and 5 (also Supplement Tab. 3 and 4). Results for all tissues are summarized and compared in Figure 3.

In order to elucidate the general relationships between  $k_3$  and other parameters across patients, scatter plots were constructed for  $k_3$  of  $TAC_{Avg}$  (tumor) versus the remaining PKA parameters as well as versus  $K_i$  and  $TBR$ , for each tissue VOI analyzed (Fig. 4); each data point represents one lesion (there is only one VOI per patient for normal lung or muscle). The corresponding Pearson correlation coefficients (R) are given in Table 6. A strong correlation was defined as  $R > 0.75$ , a weak one as  $R < 0.5$ , and all others as moderate.

For tumors'  $TAC_{Avg}$ ,  $K_1$  versus  $k_3$  results show a weak negative correlation ( $R = -0.17$ ), in contrast to what is observed for normal lung ( $R = 0.58$ ) and muscle ( $R = 0.28$ ). Additionally, Table 6 also shows R for  $k_3$  versus  $K_i$  and  $TBR$ , which are of interest as these parameters have all been proposed as possible hypoxia indices. This is supported by the degree of concordance between these parameters in tumor ( $R = 0.84$  for  $TBR-k_3$  and  $R = 0.91$  for  $K_i-k_3$ ); these correlations are highly significant ( $p < 0.001$ ). Interestingly, R is even larger ( $0.97$  and  $0.95$ ,  $p < 0.001$ ) in the case of the normal tissues studied.

Table 7 summarizes the results of voxel-wise correlations calculated between  $k_3$  and the foregoing parameters for each VOI (also Supplement Table 5). Variable voxel-wise correlations between  $K_1$  and  $k_3$  were observed for lesion VOIs ( $-0.97$ - $0.72$  and  $R < 0$  in 24 out 34 lesions, 20 of which were significant with  $p < 0.001$ ), which averaged across lesions depicts a weak inverse relationship (average  $R = -0.23 \pm 0.39$ ). For both normal tissues, R for  $K_1-k_3$  was positive for 81% of normal lung (75% with  $p < 0.05$ ) and 75% of muscle (50% with  $p < 0.05$ ) patients; 13% (lung) and 44% (muscle) of those exhibited moderate to high correlations ( $R > 0.5$ ).

The influx rate constant,  $K_i$ , which has been proposed as a surrogate measure for hypoxia, showed a positive correlation with  $k_3$  in 33 of 34 tumors, 31 of which had  $R > 0.5$  ( $p < 0.001$ ). Likewise, 100% of the patients had a  $K_i$ - $k_3$   $R > 0.5$  for normal lung and muscle. As  $k_2 \gg k_3$ , it is possible to deduce that  $K_i \cong K_1 \times k_3 / k_2$ . The highly positive correlation between  $K_i$  and  $k_3$  in all three tissue types is therefore as expected. For 71% of lesions,  $TBR$ - $k_3$  had  $R > 0$  and 53% showed moderate to strong correlations ( $p < 0.001$ ); likewise, for both normal lung and muscle tissues. Finally, 67% of lesions had non-zero FHV. Of these, 38% had  $FHV > 0.5$  (half the tumor volume).

Finally, plotting the  $K_1$ - $k_3$  voxel-wise  $R$  versus the lesion's respective average  $k_3$  shows that as the lesion becomes less hypoxic (as indicated by  $k_3$ ), the correlation between delivery and trapping becomes more positive (Fig. 5).

In order to increase the statistical power of the correlations, a similar analysis was carried by first grouping voxels into  $k_3$ -deciles using the voxel-wise parametric maps. Supplemental Fig. 1A and B show bar graphs of  $R$  for  $K_1$ - $k_3$  for the respective results from normal lung and muscle; each bar corresponds to one patient (as does the color for comparison to tumor results since several patients had multiple lesions). Supplemental Fig. 1D a similar plot for the decile-wise analysis; in this case, each bar represents a lesion (each color a patient as in A and B). Eighty-eight percent of the lesions had  $R < 0$  for  $K_1$ - $k_3$ , 59% of which had moderate to strong anti-correlations. Supplemental Fig. 1C shows the same figure for the voxel-wise results discussed in the previous section, for comparison. Figure 6 shows that as the TBR decreases, the  $R$  for  $K_1$ - $k_3$  changes from  $R < 0$  to  $R > 0$ . Similar results were found for TMR (Supplemental Fig. 2).

Finally, PKA of the  $TAC_{FHV}$  showed that for only 8/23 lesions  $k_3$  was significantly different ( $p < 0.05$ ) from that of  $TAC_{Avg}$ . Of those 8, only 5 had  $k_3$  higher than that of  $TAC_{Avg}$ . Additionally, in every case, the maximum TBR in HV was larger than the TBR for the voxel with the maximum  $k_3$ . Moreover, the maximum  $k_3$  voxel was inside the HV in 15/23 lesions.

## DISCUSSION

FMISO was first introduced as a promising hypoxia tracer because it is preferentially retained in cells with low oxygen pressure (26).  $^{18}\text{F}$ FMISO is lipophilic, diffusing passively through the cell membrane and taken up by both normoxic and hypoxic tissues. Once inside the cell, it may undergo a first reduction into R-NO<sub>2</sub>, which is reversible reaction under normoxic conditions. However, at low (hypoxic) pO<sub>2</sub>s, R-NO<sub>2</sub> is further reduced into R-NHOH, which binds to intracellular proteins, becoming irreversibly bound. Hence, there is a relationship between  $^{18}\text{F}$ FMISO trapping in cells and the degree of hypoxia. The most widely used surrogate metric of tumor hypoxia in  $^{18}\text{F}$ FMISO PET is its TBR derived from a single late time-point image. Investigators have reported times from 2-4 hrs post-FMISO administration (12,27,28). An image voxel is considered to be hypoxic if TBR exceeds a predetermined value, usually 1.2-1.4 (18,27). This approach, although simple to implement, may misidentify hypoxic voxels, a consequence of the slow  $^{18}\text{F}$ FMISO clearance from regions of high tumor perfusion. This variable uptake and slow clearance means that it is not always possible to unambiguously differentiate the impact on uptake of hypoxia and perfusion by static PET imaging alone. The acquisition of dynamic PET images combined with PKA

provides a potential methodology to distinguish delivery from trapping. This approach is more complex and acquisitions more time-consuming. Nevertheless, a few studies (15,18,21,29,30), mainly for HNCs, have demonstrated its feasibility and benefit.

In this study, we performed PKA of  $^{18}\text{F}$ MISO dynamic PET images of patients with NSCLC. All lesions investigated demonstrated uptake of  $^{18}\text{F}$ MISO and 31 of 34 studied showed some degree of irreversible trapping, i.e.  $k_3 > 0$  within the limits of the associated standard error. The generic shape of the tumor and normal lung TACs during early frames exhibits a sharp peak, reflecting the transit of the initial injection bolus through the tissue of interest, followed by the diffusion of radiotracers from the vascular compartment into the peri-vascular space.

We performed PKA of lung tumors, normal lung and muscle. The average lesion  $K_1$ , associated radio-tracer delivery, resulted in the most marked difference between these tissue types among the parameters studied. Its value was larger in tumors than in either normal lung or muscle tissue by at least a factor of 1.7 in every case (range=2 – 33,  $\mu \pm \text{SD} = 7 \pm 7$  and range=1.7 – 12,  $\mu \pm \text{SD} = 6 \pm 3$ , respectively), with a lower degree of overlap with the normal tissues than for any of the other parameters (Fig. 3B). The significantly ( $p < 0.001$ ) larger  $K_1$  values measured for lesions may reflect the abnormal tumor vasculature and easier diffusion than that of normal tissues. However, it is important to take into account that the data for normal lung has not been corrected for its lower density relative to tumor and muscle. Normal lung tissue has significant components of air and blood. As a result, activity concentration is underestimated for voxels in the parenchyma. As the air and blood fractions in the voxels are highly variable throughout the lung, corrections cannot be simply implemented via scaling.

Holman *et al*, extending the work of Lambrou, have proposed methods for voxel-wise corrections using  $CT_{Avg}$ , and showed that  $K_1$ ,  $K_i$  and  $SUV_{bw}$  were all found to be affected (31,32). Nevertheless, the method has not been validated and, thus, not applied in this study. Thus, it is expected that the values of  $K_1$  and  $K_i$  reported here for normal lung would be lower had corrections been applied.

For the two-compartment model, the rate constant  $k_3$ , representing irreversible  $^{18}\text{FMISO}$  trapping, is considered a surrogate hypoxia metric. The expectation would be that such trapping would be more significant in tumors than in normal tissues. In fact, the results in this study show that while the average lesion  $k_3$  is generally larger in tumors, there is some overlap across tissues; namely, 5 lesions had an average  $k_3$  value which was smaller than in their corresponding normal lung tissue. Three of these 5 lesions had very small values of  $k_3$  ( $< 0.001 \text{ min}^{-1}$ ), and their oxygen status might, in accordance with their trapping rate constant, be considered closer to normoxia, as expected for normal lung tissue. However, 2 of 5 patients had values of  $k_3$  in normal lung indicating unexpectedly high rates of  $^{18}\text{FMISO}$  trapping. The cause of this uptake in the normal lung tissue is unclear, and a possible consequence of lung fibrosis, inflammation or some other non-specific retention in these unhealthy patients.

Single average parameter (derived from  $TAC_{avg}$ ) comparisons may not draw clear distinctions between tissue types and lesion sub-volumes. However, it is possible to determine relationships among parameters that are indicative of the hypoxic status of tumors. The average of voxel-wise parameter correlations, Fig. 5, show that  $k_3$  increases with decreased delivery both within the tumor and across patients (30). This pattern is indicative of possible structural or functional differences between diseased



and normal tissues, leading to a fundamentally different relationship between forward transport into the metabolic compartment and  $^{18}\text{F}$ MISO trapping, as might be expected. This is further reinforced by the fact that the concordance between  $K_1$  and  $k_3$  becomes positive as  $k_3$  becomes smaller. This result may imply that the magnitude of  $R$  might be indicative of weaker trapping within the tissue due to more normoxic conditions within the tumor.

Despite the theoretical advantages of modeling dynamic PET images, there are practical difficulties that may lead to inaccuracies in the estimated parameters, beyond those associated with errors due to statistical fluctuations. The data were acquired in three parts in order to minimize patient discomfort associated with scans whose durations are greater than 45 minutes. In turn, it is necessary to co-register the two late image sets to the first in order to create one complete dynamic image series. Thus, the TAC data may contain inaccuracies due to registration errors. This effect would have a larger impact on analyses of voxel-wise TACs than of average VOI TACs. Co-registration of the FDG scan to FMISO-1 for tumor delineation and segmentation may cause further inaccuracies. Additionally, it is inevitable that there will be patient's motion during the scan, especially for FMISO-1, which we seek to minimize by use of the RT mold. However, especially in lung, breathing also introduces an additional complication. In this study, no correction for breathing motion was applied as all the lesions studied were assumed to be minimally affected by motion effects because they were either (1) very large or (2) located in regions (e.g. mediastinum or upper lung lobe) where motion is minimal. Additionally, we observed that most patients quickly fell asleep or were very

relaxed within a few minutes, leading to shallow breathing. Nevertheless, breathing motion corrections could improve the accuracy of results.

Although the current results provide evidence for the presence of hypoxic sub-volumes within each lesion, there is currently no known method for translating a value of  $k_3$  into an amount of hypoxia. Several authors have proposed TBR thresholds of 1.2-1.4 (30) as an empirical criterion for hypoxia. Twenty-three of 34 lesions studied here contained sub-volumes with  $TBR > 1.2$ , with a significant ( $p < 0.001$ ) correlation identified between TBR and the average lesion  $k_3$ . When hypoxic regions are defined solely on the basis of  $TBR > 1.2$ , more than 30% of lesions would appear to lack macroscopic areas of hypoxia. However, 81% of those are  $^{18}\text{FMISO}$  avid ( $k_3 > 0$ ,  $p < 0.05$ ), showing that TBR and  $k_3$  are not always in agreement as to determining region hypoxic. The average and maximum  $k_3$  for the latter are significantly ( $p < 0.05$ ) lower than for those lesions with HVs. Finally, voxel-wise only 52% of lesions have a significant ( $p < 0.05$ )  $R > 0.5$ .

Finally, the results presented in this paper provide further evidence that there is not always concordance between the parametric descriptors of hypoxia such as  $k_3$  and  $TBR$ . It is possible that such discrepancies are a consequence of underlying different tumor tissue pathologies such as chronic hypoxia and ribbonlike hypoxia that is observed by immunohistochemical staining (33) but not resolved by PET imaging.

## **CONCLUSION**

We have successfully performed PKA of baseline dynamic  $^{18}\text{FMISO}$  PET images in a cohort of NSCLC patients. Lesions for all patients showed evidence of hypoxia as

depicted by relatively increased  $^{18}\text{FMISO}$  concentrations, which was corroborated by the increased  $k_3$  values relative to those in normal lung and muscle. As this is a prospective study, the prognostic value of our measurements could not be assessed. This investigation demonstrates the feasibility of dynamic  $^{18}\text{FMISO}$  PET imaging in thoracic disease. In particular, future directions of this work include investigating the prognostic value of the rate constants and macro parameters derived from them.

Finally, although in this particular study we only included lesions minimally affected by motion, we are developing tools with which to implement corrections for breathing-motion of dynamic PET. This will allow us to assess the impact of breathing motion on kinetic rate constants when studying lesions in thoracic regions with significant breathing motion effects.

## **DISCLOSURE**

This study was supported by a grant from NIH/NCI U01 CA157442-3 (P.I. Sadek A. Nehmeh) and the cancer center grant P30 CA008748 (P.I. Craig B. Thompson).

## REFERENCES

1. Rosenzweig KE, Amols H, Ling CC. New radiotherapy technologies. *Semin Surg Oncol*. 2003;21:190-195.
2. Sura S, Gupta V, Yorke E, Jackson A, Amols H, Rosenzweig KE. Intensity-modulated radiation therapy (IMRT) for inoperable non-small cell lung cancer: the Memorial Sloan-Kettering Cancer Center (MSKCC) experience. *Radiother Oncol*. 2008;87:17-23.
3. Eschmann SM, Paulsen F, Reimold M, et al. Prognostic impact of hypoxia imaging with 18F-misonidazole PET in non-small cell lung cancer and head and neck cancer before radiotherapy. *J Nucl Med*. 2005;46:253-260.
4. Le QT, Chen E, Salim A, et al. An evaluation of tumor oxygenation and gene expression in patients with early stage non-small cell lung cancers. *Clin Cancer Res*. 2006;12:1507-1514.
5. Nordsmark M, Bentzen SM, Rudat V, et al. Prognostic value of tumor oxygenation in 397 head and neck tumors after primary radiation therapy. An international multi-center study. *Radiother Oncol*. 2005;77:18-24.
6. Graves EE, Vilalta M, Cecic IK, et al. Hypoxia in models of lung cancer: implications for targeted therapeutics. *Clin Cancer Res*. 2010;16:4843-4852.
7. Lee NY, Mechalakos JG, Nehmeh S, et al. Fluorine-18-labeled fluoromisonidazole positron emission and computed tomography-guided intensity-modulated radiotherapy for head and neck cancer: a feasibility study. *Int J Radiat Oncol Biol Phys*. 2008;70:2-13.
8. Das SK, Miften MM, Zhou S, et al. Feasibility of optimizing the dose distribution in lung tumors using fluorine-18-fluorodeoxyglucose positron emission tomography and single photon emission computed tomography guided dose prescriptions. *Med Phys*. 2004;31:1452-1461.
9. van Lin EN, Futterer JJ, Heijmink SW, et al. IMRT boost dose planning on dominant intraprostatic lesions: gold marker-based three-dimensional fusion of CT with dynamic contrast-enhanced and 1H-spectroscopic MRI. *Int J Radiat Oncol Biol Phys*. 2006;65:291-303.
10. Madani I, Duthoy W, Derie C, et al. Positron emission tomography-guided, focal-dose escalation using intensity-modulated radiotherapy for head and neck cancer. *Int J Radiat Oncol Biol Phys*. 2007;68:126-135.

11. Vanderstraeten B, Duthoy W, De Gerssem W, De Neve W, Thierens H. [18F]fluoro-deoxy-glucose positron emission tomography ([18F]FDG-PET) voxel intensity-based intensity-modulated radiation therapy (IMRT) for head and neck cancer. *Radiother Oncol*. 2006;79:249-258.
12. Koh WJ, Bergman KS, Rasey JS, et al. Evaluation of oxygenation status during fractionated radiotherapy in human nonsmall cell lung cancers using [F-18]fluoromisonidazole positron emission tomography. *Int J Radiat Oncol Biol Phys*. 1995;33:391-398.
13. Rajendran JG, Wilson DC, Conrad EU, et al. [(18)F]FMISO and [(18)F]FDG PET imaging in soft tissue sarcomas: correlation of hypoxia, metabolism and VEGF expression. *Eur J Nucl Med Mol Imaging*. 2003;30:695-704.
14. Rasey JS, Koh WJ, Evans ML, et al. Quantifying regional hypoxia in human tumors with positron emission tomography of [18F]fluoromisonidazole: a pretherapy study of 37 patients. *Int J Radiat Oncol Biol Phys*. 1996;36:417-428.
15. Thorwarth D, Eschmann SM, Paulsen F, Alber M. A kinetic model for dynamic [18F]-Fmiso PET data to analyse tumour hypoxia. *Phys Med Biol*. 2005;50:2209-2224.
16. Wang W, Georgi JC, Nehmeh SA, et al. Evaluation of a compartmental model for estimating tumor hypoxia via FMISO dynamic PET imaging. *Phys Med Biol*. 2009;54:3083-3099.
17. Milne EN. Circulation of primary and metastatic pulmonary neoplasms. A postmortem microarteriographic study. *Am J Roentgenol Radium Ther Nucl Med*. 1967;100:603-619.
18. Rajendran JG, Schwartz DL, O'Sullivan J, et al. Tumor hypoxia imaging with [F-18] fluoromisonidazole positron emission tomography in head and neck cancer. *Clin Cancer Res*. 2006;12:5435-5441.
19. Grunbaum Z, Freauff SJ, Krohn KA, Wilbur DS, Magee S, Rasey JS. Synthesis and characterization of congeners of misonidazole for imaging hypoxia. *J Nucl Med*. 1987;28:68-75.
20. Chapman JD, Franko AJ, Sharplin J. A marker for hypoxic cells in tumours with potential clinical applicability. *Br J Cancer*. 1981;43:546-550.
21. Wang W, Lee NY, Georgi JC, et al. Pharmacokinetic analysis of hypoxia (18)F-fluoromisonidazole dynamic PET in head and neck cancer. *J Nucl Med*. 2010;51:37-45.

22. Gupta N, Gill H, Graeber G, Bishop H, Hurst J, Stephens T. Dynamic positron emission tomography with F-18 fluorodeoxyglucose imaging in differentiation of benign from malignant lung/mediastinal lesions. *Chest*. 1998;114:1105-1111.
23. Hoekstra CJ, Hoekstra OS, Lammertsma AA. On the use of image-derived input functions in oncological fluorine-18 fluorodeoxyglucose positron emission tomography studies. *Eur J Nucl Med*. 1999;26:1489-1492.
24. Grkovski M, Schwartz J, Gonen M, et al. Feasibility of 18F-Fluoromisonidazole Kinetic Modeling in Head and Neck Cancer Using Shortened Acquisition Times. *J Nucl Med*. 2016;57:334-341.
25. Li F, Joergensen JT, Hansen AE, Kjaer A. Kinetic modeling in PET imaging of hypoxia. *Am J Nucl Med Mol Imaging*. 2014;4:490-506.
26. Rasey JS, Grunbaum Z, Magee S, et al. Characterization of radiolabeled fluoromisonidazole as a probe for hypoxic cells. *Radiat Res*. 1987;111:292-304.
27. Fleming IN, Manavaki R, Blower PJ, et al. Imaging tumour hypoxia with positron emission tomography. *Br J Cancer*. 2015;112:238-250.
28. Muzi M, Krohn KA. Imaging Hypoxia with 18F-Fluoromisonidazole: Challenges in Moving to a More Complicated Analysis. *J Nucl Med*. 2016;57:497-498.
29. Casciari JJ, Graham MM, Rasey JS. A modeling approach for quantifying tumor hypoxia with [F-18]fluoromisonidazole PET time-activity data. *Med Phys*. 1995;22:1127-1139.
30. Bruehlmeier M, Roelcke U, Schubiger PA, Ametamey SM. Assessment of hypoxia and perfusion in human brain tumors using PET with 18F-fluoromisonidazole and 15O-H<sub>2</sub>O. *J Nucl Med*. 2004;45:1851-1859.
31. Holman BF, Cuplov V, Millner L, et al. Improved correction for the tissue fraction effect in lung PET/CT imaging. *Phys Med Biol*. 2015;60:7387-7402.
32. Lambrou T, Groves AM, Erlandsson K, et al. The importance of correction for tissue fraction effects in lung PET: preliminary findings. *Eur J Nucl Med Mol Imaging*. 2011;38:2238-2246.
33. van Laarhoven HW, Kaanders JH, Lok J, et al. Hypoxia in relation to vasculature and proliferation in liver metastases in patients with colorectal cancer. *Int J Radiat Oncol Biol Phys*. 2006;64:473-482.

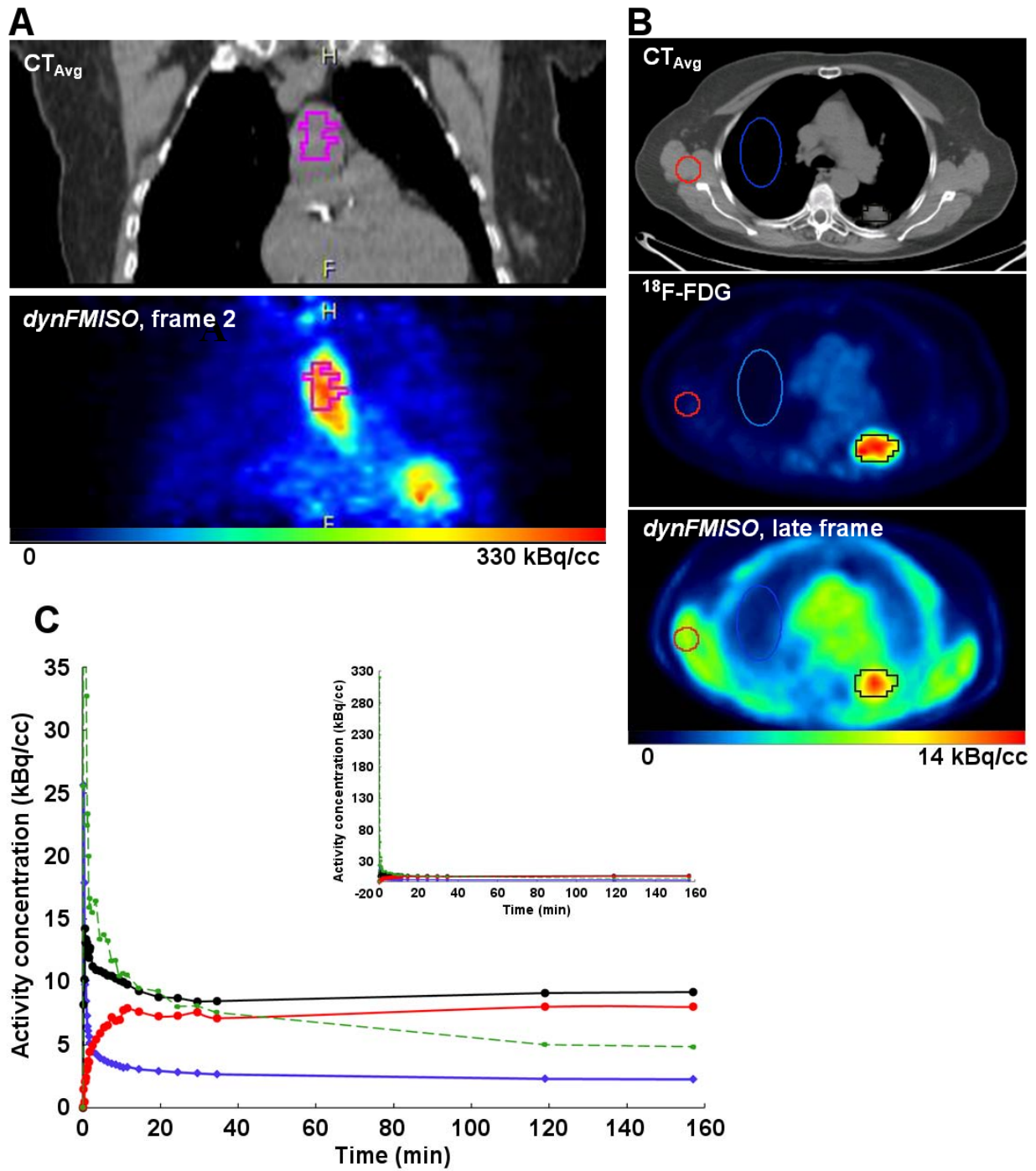


**Figure 1.** Examples of (A) aortic arch VOI and (B)  $VOI_{Tumor}$  (black),  $VOI_{Normal}$  (blue) and  $VOI_{Muscle}$  (red) (C) TACs corresponding to: IF (green),  $TAC_{Avg}$  (black),  $TAC_{Normal}$  (blue) and  $TAC_{Muscle}$  (red).

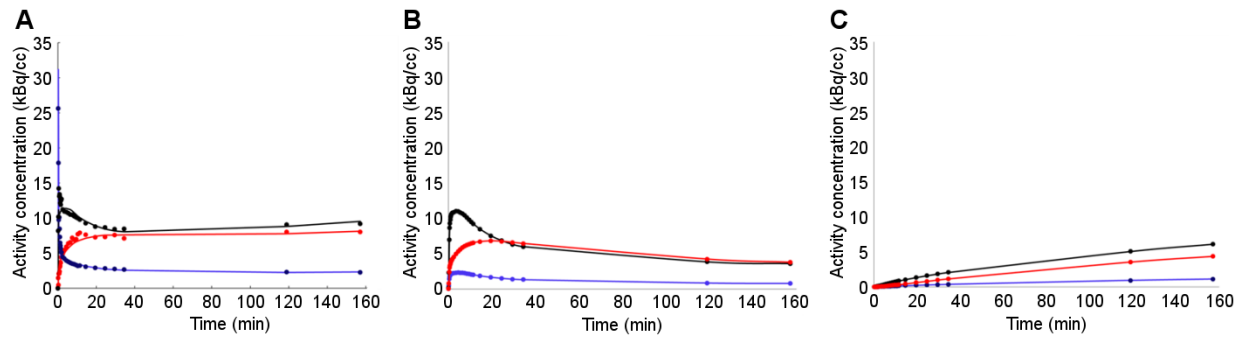


**FIGURE 2.** Total and compartment time activity curves for patient 1 VOIs determined by PKA: (A)

$C_{model}(t)$  (B)  $C_1(t)$  and (C)  $C_2(t)$  for  $TAC_{Avg}$  (black),  $TAC_{Normal}$  (blue) and  $TAC_{Muscle}$  (red).



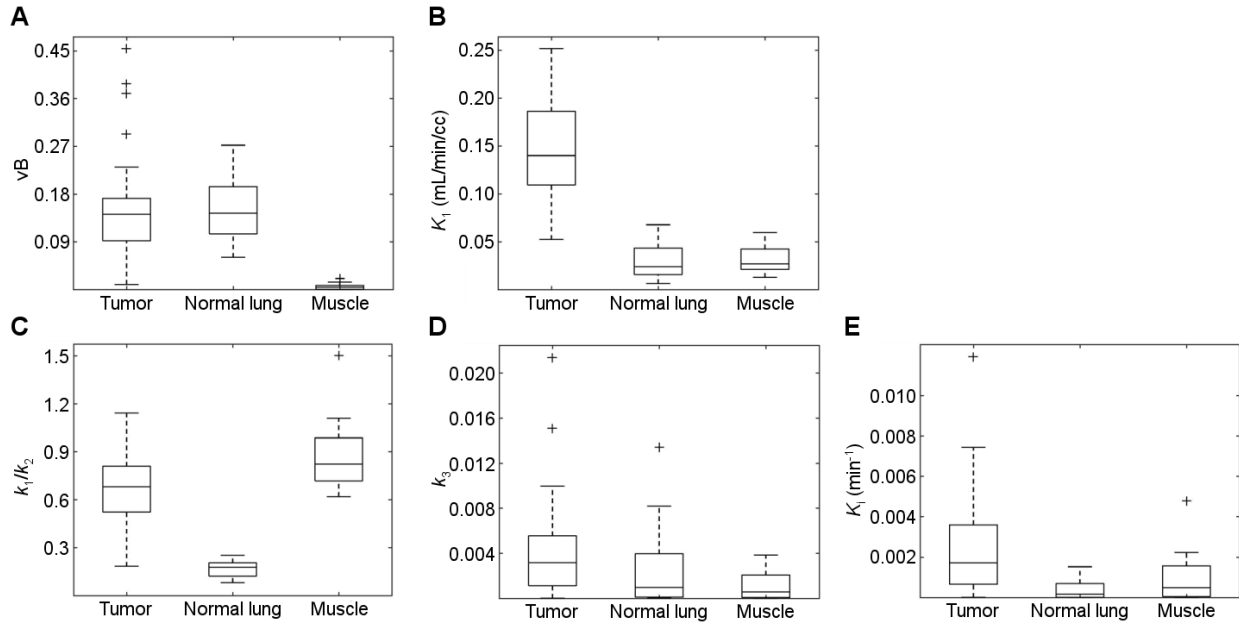


**FIGURE 3.** Comparison across tissues of parameters from PKA of  $TAC_{Avg}$  (black),  $TAC_{Normal}$  (blue) and  $TAC_{Muscle}$  (red): (A)  $vB$ , (B)  $K_1$ , (C)  $K_1/k_2$ , (D)  $k_3$ , and (E)  $K_i$ . Outliers (+) are those data farther than  $1.5 \times (Q_3 - Q_1)$  from the median (midline), where  $Q_1$  and  $Q_3$  are the data 25th and 75th percentiles, respectively.

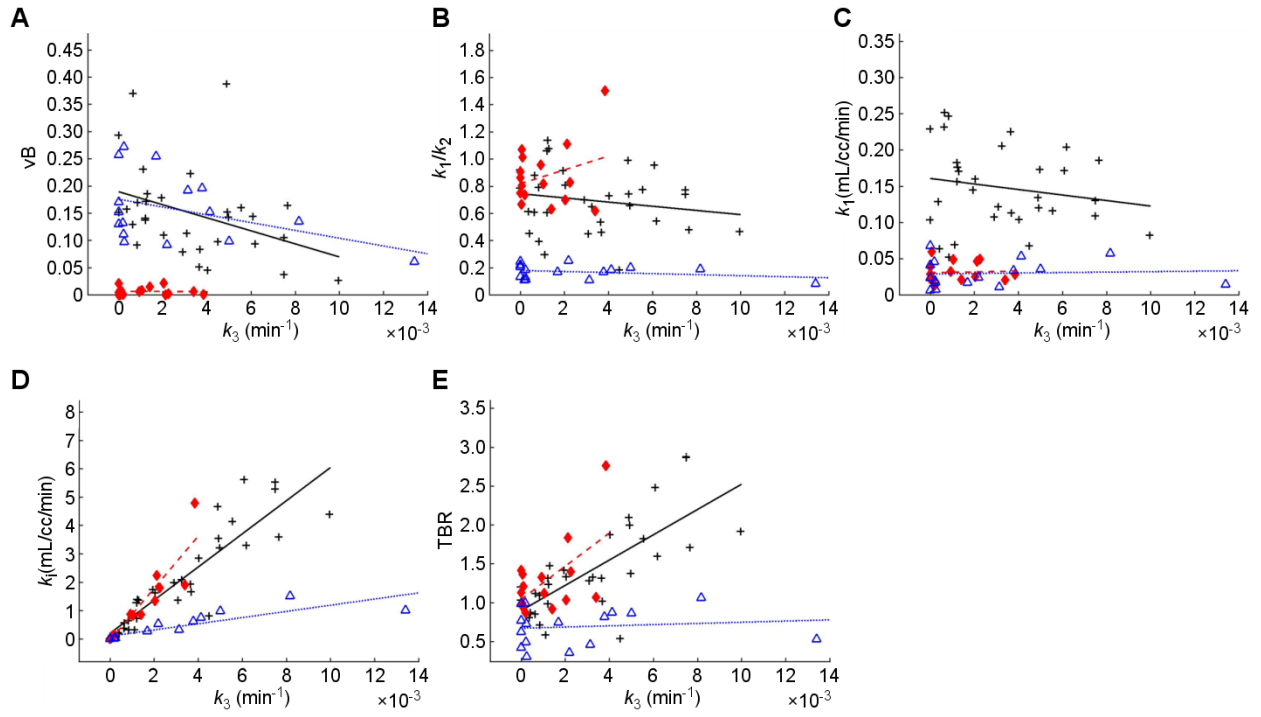


**FIGURE 4.** Scatter plots of  $k_3$  versus the: (A)  $vB$ , (B)  $K_1/k_2$ , (C)  $K_1$ , (D)  $K_i$ , and (E)  $TBR$ , for the average TACs:  $TAC_{Avg}$  (black),  $TAC_{Normal}$  (blue) and  $TAC_{Muscle}$  (red). Each point represents one lesion (some patients had multiple lesions).

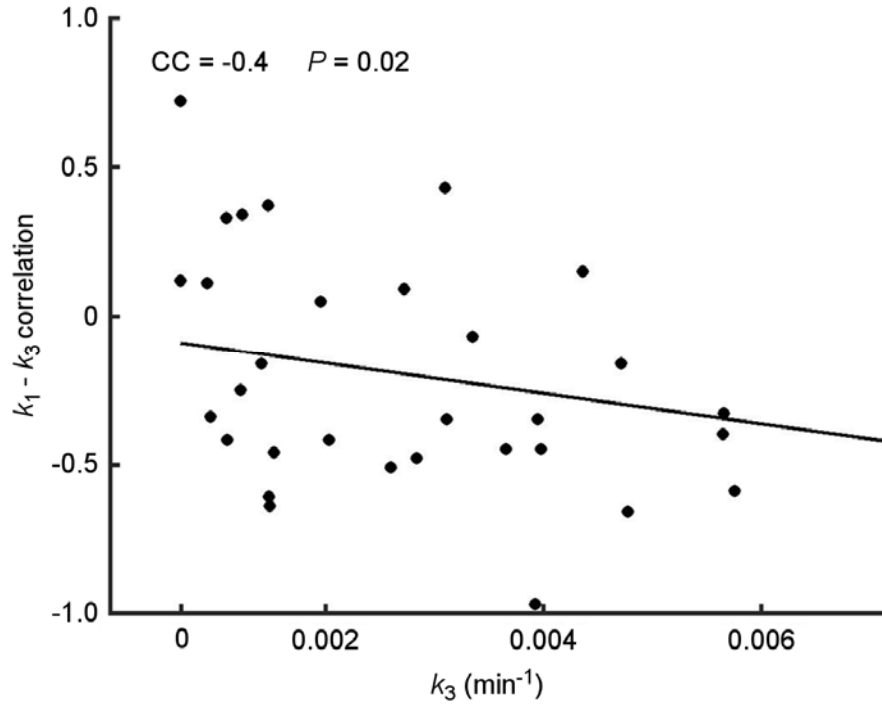


**FIGURE 5.** Scatter plot of  $K_1$ - $k_3$  voxel-wise correlation versus the average  $k_3$  in  $VOI_{Tumor}$ . Each point represents one lesion.

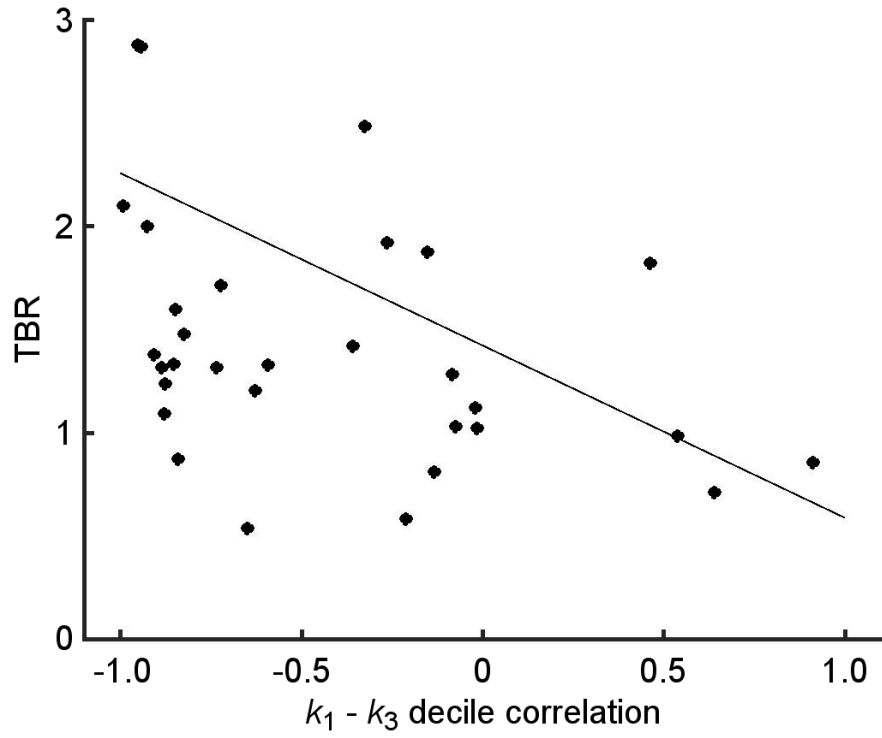


**FIGURE 6.** Scatter plot of TBR for  $VOI_{Tumor}$  vs  $K_1 - K_3$  decile correlation coefficient. Each point represents one lesion.

**TABLE 1.** Patient (P) characteristics

P	Injected Dose		Gender	Age
	MBq			
	FMISO	FDG		
1	358	435	'F'	79
2	336	419	'F'	75
3	338	411	'F'	66
4	323	426	'F'	66
5	367	395	'M'	33
6	361	419	'M'	65
7	371	429	'M'	59
8	336	462	'F'	65
9	365	441	'M'	78
10	242	441	'M'	66
11	349	430	'M'	71
12	376	429	'M'	64
13	359	437	'F'	57
14	382	415	'M'	60
15	326	450	'F'	82
16	352	432	'M'	73
<b><math>\mu \pm \sigma</math></b>	<b>346<math>\pm</math>33</b>	<b>429<math>\pm</math>16</b>		<b>66<math>\pm</math>11</b>

**TABLE 2.** Statistics of *PKA* results for average lesion TACs for each patient (*P*). See Supplement Table 1 for patient/lesion-wise results.

	vB	%SE vB	K1 (mL/min/cc)	%SE K <sub>1</sub>	K <sub>1</sub> /k <sub>2</sub>	%SE K <sub>1</sub> /k <sub>2</sub>	k <sub>3</sub> (min <sup>-1</sup> )	%SE k <sub>3</sub>	K <sub>i</sub> (mL/min/cc)	%SE K <sub>i</sub>
Average	0.15	20	0.15	11	0.69	3.4	4.1E-03	25	4.1E-03	31
σ	0.10	13	0.06	5.0	0.23	2.1	4.5E-03	27	4.5E-03	26
min	0.01	8.7	0.05	4.2	0.18	1.0	0.0E+00	5.4	0.0E+00	8.3
max	0.45	80	0.25	25	1.10	12	2.1E-02	100	2.1E-02	110

**TABLE 3. Statistics of quantitative lesion parameters for each tumor VOI and patient (P). See Supplement Table 2 for patient/lesion-wise results.**

	Maximum SUV <sub>bw</sub>	TBR	Volume (cc)	FHV
Average	3.0	1.8	19	39
$\sigma$	2.2	1.5	27	43
min	1.1	0.54	1.7	0.0
max	13	8.0	150	100

**TABLE 4.** PKA results for average normal lung TACs. See Supplement Table 3 for patient/lesion-wise results.

Normal Lung										
	vB	%SE vB	K <sub>1</sub> (mL/min/cc)	%SE K <sub>1</sub>	K <sub>1</sub> /k <sub>2</sub>	%SE K <sub>1</sub> /k <sub>2</sub>	k <sub>3</sub> (min <sup>-1</sup> )	%SE k <sub>3</sub>	Maximum SUV	TBR
<b>Average</b>	0.16	14	0.029	26	0.17	12	1.8E-03	23	1.1	0.7
<b>σ</b>	0.063	9.7	0.019	14	0.052	6.8	2.4E-03	9.3	0.5	0.2
<b>min</b>	0.064	6.2	0.0061	15	0.079	5.9	0.0E+00	12	0.4	0.3
<b>max</b>	0.27	41	0.068	71	0.25	32	8.2E-03	33	2.2	1.1



**TABLE 5.** PKA results for average muscle TACs. See Supplement Table 4 for patient/lesion-wise results.

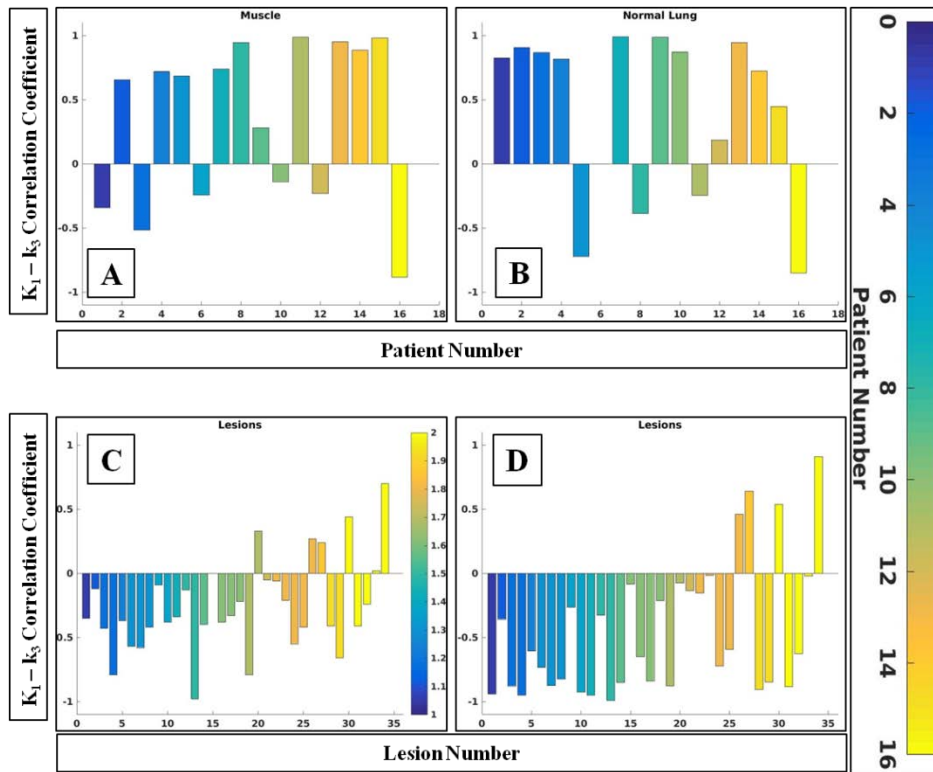
	Muscle									
	vB	%SE vB	K <sub>1</sub> (mL/min/cc)	%SE K <sub>1</sub>	K <sub>1</sub> /k <sub>2</sub>	%SE K <sub>1</sub> /k <sub>2</sub>	k <sub>3</sub> (min <sup>-1</sup> )	%SE k <sub>3</sub>	Maximum SUV	TBR
<b>Average</b>	5.9E-03	45	0.031	4.2	0.87	6.7	1.1E-03	35	1.9	1.3
<b>σ</b>	7.1E-03	57	0.013	1.5	0.22	3.5	1.3E-03	14	0.5	0.5
<b>min</b>	0.0E+00	13	0.013	2.6	0.62	2.6	0.0E+00	15	1.3	0.9
<b>max</b>	2.1E-02	200	0.059	7.5	1.5	18	3.8E-03	53	2.9	2.8

**TABLE 6.** Correlation results between  $k_3$  for average TACs and relevant parameters across patients/lesions.

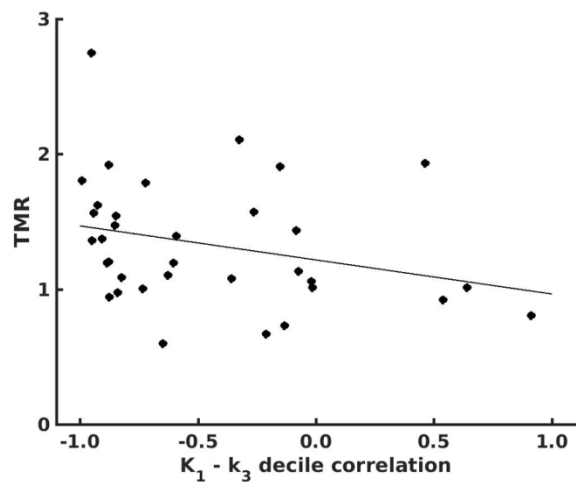
	Tumor		Normal Lung		Muscle	
	R	p-Value	R	p-Value	R	p-Value
K1 vs k3	-0.17	0.32	0.58	0.19	0.28	0.32
K1/k2 vs k3	-0.22	0.33	0.13	0.65	-0.25	0.33
TBR vs k3	0.84	<0.001	0.41	0.13	-0.05	<0.001
Ki vs k3	0.91	<0.001	0.97	<0.001	0.95	<0.001
vB vs k3	-0.38	0.036	-0.19	0.5	-0.02	0.036

**TABLE 7.** Results of voxel-wise correlation analysis. Statistics shown are determined for multiple patients and lesions. Supplement TABLE 5 for patient/lesion-wise results.

	<b>Tumor R</b>				<b>Normal Lung R</b>				<b>Muscle R</b>			
	K <sub>1</sub> -k <sub>3</sub>	K <sub>1</sub> /k <sub>2</sub> -k <sub>3</sub>	TBR-k <sub>3</sub>	K <sub>i</sub> - k <sub>3</sub>	K <sub>1</sub> - k <sub>3</sub>	K <sub>1</sub> /k <sub>2</sub> -k <sub>3</sub>	TBR-k <sub>3</sub>	K <sub>i</sub> - k <sub>3</sub>	K <sub>1</sub> - k <sub>3</sub>	K <sub>1</sub> /k <sub>2</sub> -k <sub>3</sub>	TBR-k <sub>3</sub>	K <sub>i</sub> - k <sub>3</sub>
<b>Averages</b>	-0.23	-0.42	0.26	0.70	0.29	-0.22	0.23	0.85	0.29	-0.81	0.20	0.95
<b>min</b>	0.39	0.39	0.44	0.29	0.25	0.26	0.26	0.08	0.43	0.22	0.35	0.09
<b>max</b>	-0.97	-0.97	-0.52	-0.02	-0.17	-0.64	-0.17	0.70	-0.51	-0.96	-0.36	0.64
	0.72	0.62	0.85	0.99	0.76	0.40	0.88	0.96	0.90	-0.03	0.66	1.00



**Supplemental FIGURE 1.** Bar plots of the  $K_1 - k_3$  voxel-wise R for each patient for every: (A)  $VOI_{Muscle}$ , (B)  $VOI_{Normal}$ , (C)  $VOI_{Tumor}$  and (D) using deciles of voxels in  $VOI_{Tumor}$  to increase statistical power. Each color represents an individual patient.



**Supplemental FIGURE 2.** Scatter plot of TMR for  $VOI_{Tumor}$  vs  $K_1 - k_3$  decile correlation coefficient. Each point represents one lesion.

**Supplement Table 1.** PKA results for average lesion TACs for each patient (*P*).

P	VOI	vB	%SE vB	K1 (mL/min/cc)	%SE K <sub>1</sub>	K <sub>1</sub> /k <sub>2</sub>	%SE K <sub>1</sub> /k <sub>2</sub>	k <sub>3</sub> (min <sup>-1</sup> )	%SE k <sub>3</sub>	K <sub>i</sub> (mL/min/cc)	%SE K <sub>i</sub>
1	1	0.04	23	0.13	6.4	0.77	2.5	7.50E-03	6	0.0055	11
2	1	0.18	9.8	0.14	5.7	0.91	1.8	1.90E-03	12	1.58E-04	15
3	1	0.06	42	0.21	14	0.59	4	2.10E-02	7.2	2.92E-03	21
	2	0.01	80	0.13	9.3	0.52	3.2	1.50E-02	5.6	2.68E-03	14
4	1	0.08	19	0.11	6.8	0.7	2.4	2.90E-03	12	2.42E-04	16
5	1	0.14	24	0.16	11	1.1	3.5	1.20E-03	33	3.64E-05	37
	2	0.17	20	0.18	9.8	1.1	3.1	1.20E-03	28	4.29E-05	31
	3	0.19	27	0.17	8.7	1.1	3.2	1.30E-03	7.1	1.83E-04	15
6	1	0.03	17	0.08	11	0.47	3.2	1.00E-02	10	1.00E-03	18
	2	0.15	8.7	0.12	4.2	0.74	1.7	4.90E-03	5.6	8.75E-04	8.3
7	1	0.10	16	0.11	7	0.74	2.3	7.50E-03	6.9	1.09E-03	12
8	1	0.14	11	0.17	11	0.96	3.7	6.10E-03	12	5.08E-04	20
	2	0.39	15	0.13	7.7	0.99	2	4.90E-03	13	3.77E-04	17
9	1	0.11	14	0.16	8.7	0.81	2.7	2.00E-03	10	2.00E-04	16
10	1	0.11	26	0.12	25	0.45	12	3.10E-03	19	1.63E-04	42
	2	0.10	8.8	0.07	21	0.18	7.9	4.50E-03	100	4.50E-05	100
	3	0.45	11	0.06	15	0.45	6.9	4.20E-04	28	1.50E-05	36
	4	0.23	13	0.07	4.6	0.3	1	1.10E-03	16	6.88E-05	17
11	1	0.09	23	0.25	11	0.79	2.4	8.20E-04	100	8.20E-06	100
	2	0.15	10	0.23	6.7	0.92	1.8	0.00E+00	48	1.00E-08	49
12	1	0.16	21	0.13	7.2	0.61	2.7	3.60E-04	10	3.60E-05	15
13	1	0.05	18	0.10	11	0.73	3.1	4.00E-03	12	3.33E-04	20
	2	0.08	15	0.11	13	0.46	3.6	3.70E-03	8.3	4.46E-04	20
	3	0.16	17	0.19	14	0.48	3.3	7.60E-03	13	5.85E-04	24
	4	0.22	13	0.21	8.4	0.65	2.7	3.30E-03	8.8	3.75E-04	15
	5	0.16	16	0.12	16	0.78	5.4	5.50E-03	56	9.82E-05	61
14	1	0.17	16	0.05	11	0.39	2.7	8.50E-04	15	5.67E-05	22
15	1	0.14	14	0.17	8.1	0.66	1.9	5.00E-03	6.3	7.94E-04	13
	2	0.09	14	0.20	8.5	0.54	2	6.20E-03	15	4.13E-04	19
16	1	0.14	16	0.18	6.8	0.61	1.5	1.20E-03	5.4	2.22E-04	11
	2	0.05	27	0.23	23	0.54	5.5	3.60E-03	100	3.60E-05	110
	3	0.29	14	0.10	15	0.79	2.9	0.00E+00	46	1.04E-22	51
	4	0.37	29	0.25	17	0.88	3.8	6.50E-04	47	1.38E-05	53
	5	0.13	21	0.23	12	0.61	3.4	6.30E-04	30	2.10E-05	35
	Average	0.15	20	0.15	11	0.69	3.4	4.1E-03	25	4.1E-03	31
	σ	0.10	13	0.06	5.0	0.23	2.1	4.5E-03	27	4.5E-03	26
	min	0.01	8.7	0.05	4.2	0.18	1.0	0.0E+00	5.4	0.0E+00	8.3
	max	0.45	80	0.25	25	1.10	12	2.1E-02	100	2.1E-02	110

**Supplement Table 2.** Quantitative lesion parameters for each tumor VOI and patient (P).

P	VOI Number	Maximum SUV <sub>bw</sub>	TBR	Volume (cc)	FHV
1	1	2.7	2.9	26	94
2	1	2.0	1.4	6.7	57
3	1	4.2	5.2	21	100
	2	3.2	4.0	13	100
4	1	13	8.0	5.2	100
5	1	2.3	1.3	2.7	50
	2	2.1	1.2	17	2.3
	3	2.6	1.5	19	43
6	1	2.5	1.9	17	100
	2	2.6	2.0	32	100
7	1	3.7	2.9	150	94
8	1	3.5	2.5	5.1	100
	2	3.0	2.1	7.6	100
9	1	2.2	1.3	64	19
10	1	2.5	1.3	28	2.1
	2	1.1	0.54	5.2	0.0
	3	1.7	0.87	8.8	0.0
	4	1.2	0.58	2.8	0.0
11	1	1.9	1.1	11	0.0
	2	1.8	1.0	2.3	0.0
12	1	2.1	0.81	2.8	0.0
13	1	5.8	1.9	11	63
	2	3.1	1.0	1.7	0.0
	3	5.3	1.7	5.6	53
	4	4.1	1.3	8.0	12
	5	5.6	1.8	8.2	95
14	1	1.6	0.71	52	0.0
15	1	2.3	1.4	22	11
	2	2.7	1.6	17	29
16	1	1.4	0.98	3.7	0.0
	2	1.9	1.3	7.7	6.3
	3	1.7	1.2	33	0.34
	4	1.6	1.1	20	0.0
	5	1.2	0.85	6.7	0.0
	Average	3.0	1.8	19	39
	$\sigma$	2.2	1.5	27	43
	min	1.1	0.54	1.7	0.0
	max	13	8.0	150	100

**Supplementary TABLE 3.** PKA results for average normal lung TACs.

Normal Lung										
Patient	vB	%SE vB	K <sub>1</sub> (mL/min/cc)	%SE K <sub>1</sub>	K <sub>1</sub> /k <sub>2</sub>	%SE K <sub>1</sub> /k <sub>2</sub>	k <sub>3</sub> (min <sup>-1</sup> )	%SE k <sub>3</sub>	Maximum SUV	TBR
1	0.098	Inf	0.035	15	0.20	6.9	5.0E-03	13	0.8	0.9
2	0.20	Inf	0.033	17	0.17	9.2	3.8E-03	16	1.1	0.8
3	0.13	33	0.057	39	0.19	20	8.2E-03	26	0.8	1.1
4	0.15	12	0.023	17	0.25	6.7	0.0E+00	Inf	1.7	1.0
5	0.26	14	0.068	36	0.21	18	0.0E+00	Inf	1.1	0.6
6	0.064	7.7	0.0098	16	0.079	6.9	1.3E-04	Inf	0.6	0.5
7	0.097	11	0.0072	17	0.11	7.9	2.5E-04	12	0.4	0.3
8	0.15	7.7	0.053	31	0.19	13	4.1E-03	27	1.0	0.9
9	0.19	Inf	0.011	24	0.11	11	3.1E-03	Inf	0.7	0.5
10	0.17	17	0.041	16	0.22	6.3	0.0E+00	33	1.2	0.8
11	0.092	6.2	0.024	21	0.25	9.5	2.2E-03	33	0.6	0.4
12	0.25	Inf	0.017	25	0.17	10	1.7E-03	Inf	1.9	0.7
13	0.27	Inf	0.017	27	0.19	13	2.2E-04	Inf	2.2	0.7
14	0.13	6.6	0.0061	20	0.13	5.9	0.0E+00	Inf	0.8	0.4
15	0.13	14	0.046	25	0.11	11	1.8E-04	Inf	1.6	1.0
16	0.11	Inf	0.019	71	0.13	32	2.2E-04	Inf	0.7	0.5
<b>Average</b>	0.16	14	0.029	26	0.17	12	1.8E-03	23	1.1	0.7
<b>σ</b>	0.063	9.7	0.019	14	0.052	6.8	2.4E-03	9.3	0.5	0.2
<b>min</b>	0.064	6.2	0.0061	15	0.079	5.9	0.0E+00	12	0.4	0.3
<b>max</b>	0.27	41	0.068	71	0.25	32	8.2E-03	33	2.2	1.1

**Supplementary TABLE 4.** PKA results for average muscle TACs.

Patient	Muscle									TBR
	vB	%SE vB	K <sub>1</sub> (mL/min/cc)	%SE K <sub>1</sub>	K <sub>1</sub> /k <sub>2</sub>	%SE K <sub>1</sub> /k <sub>2</sub>	k <sub>3</sub> (min <sup>-1</sup> )	%SE k <sub>3</sub>	Maximum SUV	
1	0.0E+00	Inf	0.046	5.4	1.1	7.9	2.1E-03	38	1.7	1.8
2	5.8E-04	Inf	0.059	6.1	1.1	18	6.8E-05	52	1.9	1.4
3	2.5E-04	24	0.028	3.4	1.5	8.6	3.8E-03	Inf	2.2	2.8
4	7.9E-03	30	0.021	3.2	1.0	4.6	9.9E-05	44	2.0	1.2
5	6.0E-03	200	0.032	5.6	0.96	4.4	9.3E-04	20	2.3	1.3
6	1.4E-03	20	0.049	4.7	0.83	5.9	2.3E-03	26	1.6	1.4
7	2.1E-02	28	0.025	3.0	0.70	6.0	2.0E-03	Inf	1.3	1.0
8	4.2E-03	59	0.022	7.5	0.86	9.4	0.0E+00	Inf	1.6	1.4
9	4.5E-03	Inf	0.023	5.8	0.67	7.2	5.5E-05	Inf	1.6	1.0
10	0.0E+00	20	0.028	4.5	0.75	6.3	0.0E+00	53	1.7	1.1
11	1.4E-02	35	0.021	4.3	0.63	3.4	1.4E-03	36	1.6	0.9
12	7.5E-03	Inf	0.049	3.0	0.82	5.5	1.0E-03	Inf	2.9	1.1
13	0.0E+00	Inf	0.021	2.7	0.80	7.2	6.5E-05	Inf	2.9	0.9
14	0.0E+00	13	0.013	2.8	0.74	2.6	2.0E-04	Inf	1.7	0.9
15	2.1E-02	18	0.039	2.6	0.90	4.1	0.0E+00	15	1.6	1.0
16	5.6E-03	Inf	0.020	3.1	0.62	5.6	3.4E-03	Inf	1.5	1.1
<b>Average</b>	5.9E-03	45	0.031	4.2	0.87	6.7	1.1E-03	35	1.9	1.3
<b>σ</b>	7.1E-03	57	0.013	1.5	0.22	3.5	1.3E-03	14	0.5	0.5
<b>min</b>	0.0E+00	13	0.013	2.6	0.62	2.6	0.0E+00	15	1.3	0.9
<b>max</b>	2.1E-02	200	0.059	7.5	1.5	18	3.8E-03	53	2.9	2.8



**Supplemental TABLE 5.** Results of the voxelwise correlation between  $K_1$  and  $k_3$ .

P	VOI	Tumor		Normal Lung		Muscle	
		R	p-Value	R	p-Value	R	p-Value
1	1	-0.40	<0.001	0.37	<0.001	-0.23	<0.001
2	1	0.05	0.68	0.38	<0.001	0.38	0.06
3	1	-0.48	<0.001	0.19	<0.001	-0.14	0.23
	2	-0.80	<0.001				
4	1	-0.51	<0.001	0.35	<0.001	0.53	<0.001
5	1	-0.61	<0.001	0.04	0.17	0.32	<0.001
	2	-0.64	<0.001				
	3	-0.46	<0.001				
6	1	-0.25	<0.001	0.02		-0.14	0.16
	2	-0.35	<0.001				
7	1	-0.33	<0.001	0.24	<0.001	0.56	<0.001
8	1	-0.16	0.26	-0.08	<0.001	0.82	<0.001
	2	-0.97	<0.001				
9	1	-0.42	<0.001	0.61		0.29	<0.001
10	1	0.09	0.15	0.41	<0.001	-0.08	0.92
	2	-0.45	<0.001				
	3	-0.34	<0.001				
	4	-0.16	0.46				
11	1	-0.25	0.01	-0.17	<0.001	0.90	<0.001
	2	0.12	0.59				
12	1	0.11	0.61	0.30	<0.001	-0.01	0.88
13	1	-0.07	0.45	0.50	<0.001	0.87	<0.001
	2	-0.35	0.18				
	3	-0.59	<0.001				
	4	-0.48	<0.001				
	5	0.15	0.17				
14	1	0.34	<0.001	0.44	<0.001	0.42	<0.001
15	1	-0.45	<0.001	0.30	<0.001	0.67	<0.001
	2	-0.66	<0.001				
16	1	0.37	<0.001	-0.04	0.12	-0.51	<0.001
	2	-0.42	<0.001				
	3	0.33	<0.001				
	4	0.43	<0.001				
	5	0.72	<0.001				
	Average	-0.23		0.34		0.58	
	$\sigma$	0.39		0.15		0.23	
	min	-0.97		-0.17		-0.51	
	max	0.72		0.61		0.90	